Available online at www.sciencedirect.com

ScienceDirect

Acta Materialia 74 (2014) 125–131

Acta MATERIALIA

www.elsevier.com/locate/actamat

Predicting structure and energy of dislocations and grain boundaries

Chen Shen [a], Ju Li [b,c], Yunzhi Wang [d,*]

[a] GE Global Research, One Research Circle, Niskayuna, NY 12309, USA
[b] Department of Nuclear Science and Engineering, Massachusetts Institute of Technology, 77 Massachusetts Avenue, Cambridge, MA 02139, USA
[c] Department of Materials Science and Engineering, Massachusetts Institute of Technology, 77 Massachusetts Avenue, Cambridge, MA 02139, USA
[d] Department of Materials Science and Engineering, Ohio State University, 2041 College Road, Columbus, OH 43210, USA

Received 14 November 2013; received in revised form 21 March 2014; accepted 29 March 2014
Available online 10 May 2014

Abstract

A microscopic phase field (MPF) model is formulated to describe quantitatively the core structure and energy of dislocations using *ab initio* data as input. Based on phase field microelasticity theory implemented in the slip plane using Green's function to describe the long-range elastic interaction, the MPF model is a three-dimensional generalization of the Peierls model. Using the same generalized stacking fault energy as input, the core structure and energy predicted for straight dislocations by the MPF model show complete agreement with those predicted by the Peierls model. The ability of the MPF model to treat dislocations of arbitrary configurations is demonstrated by calculating the structure and energy of a twist grain boundary in aluminum. After discrete lattice sampling a la Nabarro, the grain boundary energy manifests Read–Shockley behavior for low-angle boundaries as well as deep cusps for high-angle special boundaries, indicating a "Peierls torque friction" effect for grain boundaries that has the same physical origin as the Peierls lattice friction for dislocation cores.

Keywords: Core structure; Defect; Aluminum; Peirels model; Phase field method

1. Introduction

Dislocations and grain boundaries (GBs) are fundamental structural defects that dictate the physical and mechanical properties of crystalline solids [1,2]. Defect engineering, where dislocation configurations and grain boundary characters are optimized to achieve specific properties or functionalities, relies on knowledge of the fundamental properties of these defects. Even after decades of research since the discovery of dislocations in the 1930s, predicting their basic properties (e.g. structure, energy and chemistry of a dislocation core) still poses a great challenge [3–13]. While *ab initio* calculations and MD simulations are powerful tools for studying GBs and dislocations, they are limited by the size scale (for example, the low-angle GBs studied in this paper have very large unit cells) and by the complexities of the interactions that they can handle, including chemical composition and timescale. For example, empirical interatomic potentials are typically hard stretched to handle more than two element types. *Ab initio* calculations, while not limited in the element types, are much more limited in size scale, and would also be hard pressed to describe finite-temperature behavior because of timescale limitations.

Because of these limitations, the most widely used methods today in studying dislocations are still based on continuum elasticity. There are two classes of approach to dislocations: the Volterra model [14] and the Peierls model [15] (see also Ref. [16] for a recent review). In the Volterra model, a dislocation is treated as a geometrical line singularity in a linear elastic continuum, so dealing

* Corresponding author. Tel.: +1 614 292 0682; fax: +1 614 292 1537.
E-mail address: wang.363@osu.edu (Y. Wang).

http://dx.doi.org/10.1016/j.actamat.2014.03.065
1359-6454/

with atomic displacements at the very core of the dislocation is avoided. As a result, the size (cut-off radius) and energy associated with a dislocation core are inputs rather than outputs of the model. Discrete dislocation (DD) simulations [17–24], which are mostly based on the Volterra framework, require the definition of the cut-off radius for dislocation cores and the rules for core–core reactions and junction formation. In the Peierls model, on the other hand, a dislocation core is treated by two competing energetic terms: a non-quadratic energy from materials residing in the slipped region, described by the generalized stacking fault (GSF) energy [25–28], which has non-convex parts, and a quadratic elastic energy from materials in the remaining crystal volume. The elastic energy term alone favors an infinitely extended dislocation core, while the inelastic non-convex energy term favors an infinitely contracted core. The interplay of the two yields an equilibrium core structure with a finite size and the associated core energy. The inelastic energy in the Peierls model is a much reduced (1-D [29] or 2-D [25]) section of a general potential energy surface defined in a $3N$-dimensional configurational space (where N is the total number of atoms). In principle, the critical information about core–core interactions required by the DD simulations can be obtained from the Peierls model. The calculation of the elastic energy in the Peierls model, however, employs a dislocation density infinite ribbon to infinite ribbon interaction kernel of $\log r$ type, which limits its applications to straight dislocations.

The phase field model for dislocations [30] employs the Khachaturyan–Shatalov (KS) microelasticity theory [31–33], implemented using the exact 3-D Green function, to describe the long-range elastic interaction. The volume element to volume element interaction kernel of $1/r^3$ type is more general than the previous $\log r$-type interaction kernel. For straight dislocations, these two integrals give exactly the same elastic energy. However, when the symmetry is broken in the dislocation line direction, the $\log r$ kernel no longer works, but the phase field energy functional continues to work as demonstrated [30,34].

However, because of the coarse-grained (10–100b, b as Burgers vector) nature of the method, there has been no rigorous treatment of dislocation cores in these approaches. The incorporation of the GSF energy into the phase field model [34,35] has made it possible to treat dislocation core structures at the sub-Burgers vector resolution, as in the Peierls model, but the predicted core structure by the phase field model [35] still does not converge exactly to the Peierls model. In this paper we formulate a new approach, called the microscopic phase field (MPF) model, taking full advantage of the KS microelasticity theory mentioned above, and show its equivalence to the Peierls model when describing straight dislocations. We then demonstrate the ability of the MPF model to treat more complex dislocation core configurations, such as those seen in GB dislocation networks. Being a 3-D generalization of the Peierls model, the MPF model offers a general quantitative means of predicting the defect size, energy and activation pathway associated with defect nucleation, as well as treating dislocation core–core interactions using *ab initio* electronic structure calculations as input.

In previous phase field dislocation models [30,34,35], the inelastic displacement or strain fields are defined and relaxed in the 3-D space. The local energy density in any volume element is composed of an elastic energy and a crystalline (or GSF) energy. Since, by definition, the crystalline energy reduces to the elastic energy at a small strain value, there is a possible overcounting in the total energy. The Peierls model, on the other hand, does not have this ambiguity since it treats the two energies in separate space: an atomic-layer thin slip plane, where the displacement is inelastic and is treated by a non-convex (the GSF) energy, and the remaining space as a linear elastic body fully described by the quadratic elastic energy. In the present model we formulate a new elasticity expression that, similar to the treatment in the Peierls model, confines the inelastic displacement strictly to the slip plane and resides the elastic energy in the two infinite half spaces. This, together with further removal of the gradient energy term, allows the MPF model to converge to the Peierls model.

The MPF model has a spatial resolution of dislocation core size, similar to the Peierls model. At such a length scale, as discussed earlier, the equilibrium core width is balanced by the elastic energy and the inelastic misfit energy. This is different from the mesoscale phase field dislocation models, where a conventional gradient energy is required to produce a smooth (though artificially wide, mesoscale size) dislocation core. However, a gradient term with distinct physical meaning could still be present at the microscopic scales. For example, a typical gradient form was shown in a continuum transition from a lattice Greens function formulation for Peierls dislocation [36]. Such a form was also found in the transition of a discrete spinodal decomposition model [37] to a continuum one [38] in phase transformation theory. More discussions may be found in Ref. [16].

2. Microscopic phase field dislocation model

In the Peierls model, a dislocation is described by a 1-D spatially continuous distribution of (inelastic) slip displacement traversing a dislocation core. The displacement, mostly local to the core, results in an atomic misfit energy to the crystal, due to local disregistry of atomic positions above and below the slip plane, and a long-range elastic energy. Such a picture can be generalized to a field description of strain field. This results in the basic order parameter in the MPF dislocation model, $\epsilon_{ij}(\mathbf{r})$, defined as an inelastic strain field with reference to a perfect crystal. It is expressed as

$$\epsilon_{ij}(\mathbf{r}) = \sum_{p=1}^{N} \epsilon_{ij}^{p} \eta_p(\mathbf{r}) \tag{1}$$

over all active slip systems, each characterized by a phase field η_p and an associated unit (slip type) strain tensor

$$\epsilon_{ij}^p = \frac{n_i^p b_j^p + n_j^p b_i^p}{2d^p} \tag{2}$$

Here p is the index for each of the N slip systems, and $\mathbf{b}^p$, $\mathbf{n}^p$ and d^p are the respective Burgers vector, slip plane's normal vector and interplanar distance of the slip planes.

The inelastic strain field fully describes the configuration of dislocations. It gives rise to the total energy as a functional

$$E = E[\epsilon_{ij}(\mathbf{r})] = E^m + E^{el} + W \tag{3}$$

The elastic energy

$$E^{el} = \frac{1}{2}\fint\left[C_{ijkl}\tilde{\epsilon}_{ij}(\mathbf{g})\tilde{\epsilon}_{kl}^*(\mathbf{g}) - n_i\tilde{\sigma}_{ij}(\mathbf{g})\Omega_{jk}(\mathbf{n})\tilde{\sigma}_{kl}^*(\mathbf{g})n_l\right]\frac{\mathrm{d}\mathbf{g}}{(2\pi)^3} \tag{4}$$

with $\mathbf{g}$ the reciprocal vector, $\mathbf{n} \equiv \mathbf{g}/|\mathbf{g}|$ its direction and $[\Omega]_{ik}^{-1}(\mathbf{n}) = C_{ijkl}n_jn_l$. The tilde $\sim$ designates a Fourier transform, and the asterisk a complex conjugation. $\sigma_{ij} \equiv C_{ijkl}\epsilon_{kl}$. The principal value integral $\fint$ excludes a small volume $2\pi/V$ at $\mathbf{g} = 0$, with V the volume of the system in the real space. With Eq. (1), the elastic energy becomes

$$E^{el} = E^{el}[\eta(\mathbf{r})] = \frac{1}{2}\sum_{p,q=1}^{N}\fint B_{pq}(\mathbf{n})\tilde{\eta}_p(\mathbf{g})\tilde{\eta}_q^*(\mathbf{g})\frac{\mathrm{d}\mathbf{g}}{(2\pi)^3} \tag{5}$$

where $B_{pq}(\mathbf{n}) = C_{ijkl}\epsilon_{ij}^p\epsilon_{kl}^q - n_i\sigma_{ij}^p\Omega_{jk}(\mathbf{n})\sigma_{kl}^q n_l$. The crystalline energy is

$$E^m = \int f^m(\epsilon_{ij}(\mathbf{r}))\,\mathrm{d}\mathbf{r} \tag{6}$$

and the mechanical work is

$$W = -\int \sigma_{ij}^{appl}(\mathbf{r})\epsilon_{ij}(\mathbf{r})\,\mathrm{d}\mathbf{r} \tag{7}$$

with applied stress σ_{ij}^{appl}.

We now consider that $\eta(\mathbf{r})$ is only distributed in a plane $z = z_s$, which coincides with the slip plane, i.e.

$$\eta_p(\mathbf{r}) = \phi_p(x,y)\delta(z - z_s)d \tag{8}$$

with d the inter-planar spacing, and $\phi_p(x,y) \equiv \eta_p(x,y,z_s)$. The elastic energy (5) becomes

$$E^{el} = \frac{1}{2}\sum_{p,q=1}^{N}\int\int \Lambda_{pq}(g_x,g_y)\tilde{\phi}_p(g_x,g_y)\tilde{\phi}_q^*(g_x,g_y)\frac{\mathrm{d}g_x\mathrm{d}g_y}{(2\pi)^2} \tag{9}$$

with

$$\Lambda_{pq}(g_x,g_y) \equiv d^2\int B_{pq}(\mathbf{n})\frac{\mathrm{d}g_z}{2\pi} \tag{10}$$

Note that, while B_{pq} is only a function of direction $\mathbf{n}$ in the reciprocal space, Λ_{pq} is generally not. The crystalline energy becomes

$$E^m = \int \frac{\gamma(\mathbf{u}(\mathbf{r}))}{d}\,\mathrm{d}\mathbf{r} = \int \gamma(\mathbf{u}(\mathbf{r}))\,\mathrm{d}x\,\mathrm{d}y \tag{11}$$

with γ the GSF energy [25]. In the plane, the independent variable ϵ_{ij} reduces to the inelastic displacement vector $\mathbf{u}(\mathbf{r}) \equiv \sum_{p=1}^{N}\mathbf{b}^p\phi_p(\mathbf{r})$. It follows that

$$\begin{aligned}\frac{\delta E}{\delta\phi_p} &= d\delta(z - z_s)\frac{\delta E}{\delta\eta_p}\\ &= \frac{\partial\gamma}{\partial\phi_p} - d\sigma_{ij}^{appl}(\mathbf{r})\epsilon_{ij}^0\\ &\quad + \sum_{q=1}^{N}\int\int \Lambda_{pq}(g_x,g_y)\tilde{\phi}_q(g_x,g_y)e^{i(g_xx+g_yy)}\frac{\mathrm{d}g_x\mathrm{d}g_y}{(2\pi)^2}\end{aligned} \tag{12}$$

The dislocation dynamics is characterized by a linearized dissipative law:

$$\frac{\partial\phi_p}{\partial t} = -L_p\frac{\delta E}{\delta\phi_p} \tag{13}$$

The special condition, $\delta E/\delta\phi_p = 0$, corresponds to an equilibrium state of a dislocation (or dislocations).

Eqs. (1)–(13) are analytically similar to common phase field microelasticity for alloy precipitates [33], with one important distinction: the order parameter fields reside in a plane (the crystallographic slip plane) instead of a 3-D space. Therefore, it is particularly efficient to employ a numerical scheme based on 2-D spatial discretization and fast Fourier transform (FFT), rather than the more general 3-D discretization and FFT for treating precipitates. In essence, because a general dislocation loop may be regarded as an infinitely thin precipitate, one can employ 2-D FFT to resolve the area element to area element elastic interaction mediated by a 3-D elastic half space (the bottom elastic half space is anti-symmetric to the top elastic half space, and the two half spaces are "glued" together by the nonlinear, nonconvex GSF). This linear elastic interaction is long ranged, but is convex and additive, and therefore best handled in 2-D reciprocal space (although the Green's function itself is derived from 3-D elasticity). The nonlinear nonconvex GSF that glues the two half spaces together provides the nonlinearity in this problem for "phase transformation" in the slip order parameter; it is local and therefore best handled in 2-D real space.

We apply Eq. (13) to calculate dissociation of a $\langle 1\,1\,0\rangle$ dislocation in Ni_3Al that Schoeck et al. [7] did with a Peierls model. The same GSF energy γ and anisotropic elastic constants are used. As shown in Fig. 1, the core structures calculated from Eq. (12) (smooth curves) agree with those from the Peierls model (open and filled circles). It is also seen that, as Schoeck et al. had shown, the core configurations do not strictly pass the planar faults CSF and APB on the GSF energy surface because of the elastic stress, with the screw core deviating further due to the greater self-stress.

3. Pure-screw twist boundary

With a field description of inelastic displacement $\mathbf{u}(\mathbf{r})$, a dislocation is seen not as a singular line with a unit Burgers vector, but as a distributed configuration; nor is this description restricted to simple geometries such as straight lines. With the latter, the model is superior for treating complex dislocation configurations, for example, a pure-screw

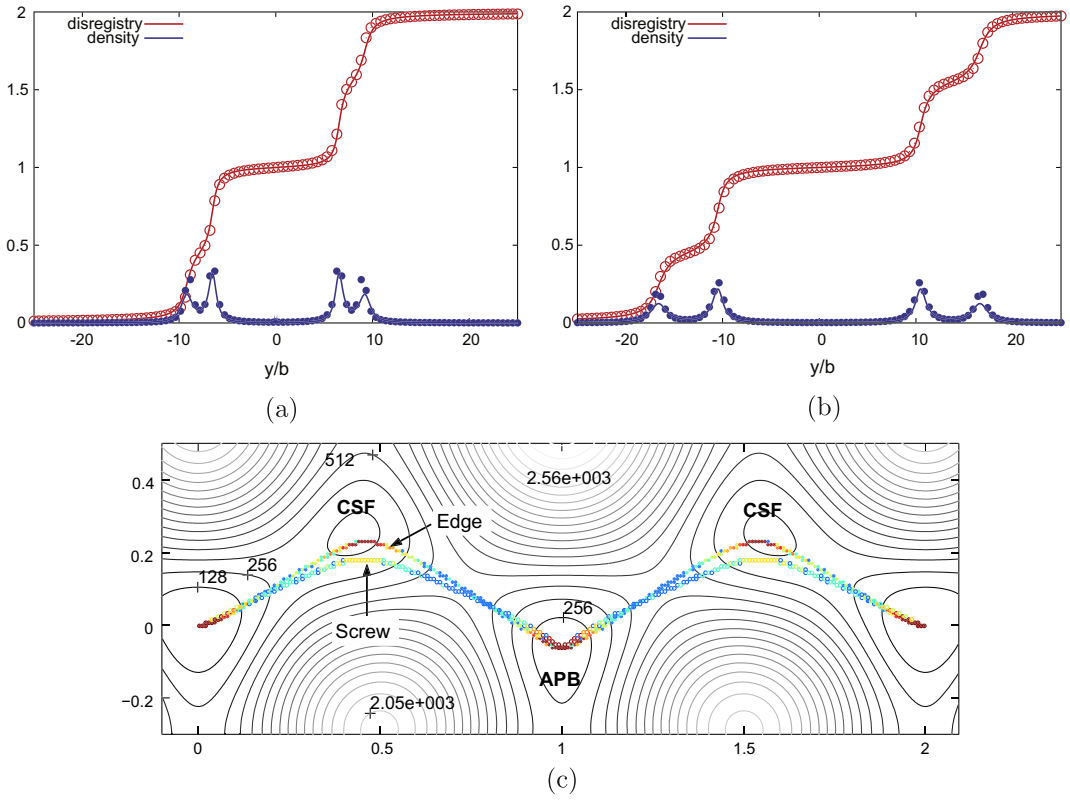

Fig. 1. The fourfold core structure of the $\langle 1\,1\,0\rangle$ super-dislocation of (a) screw and (b) edge types in Ni_3Al. Lines are from the current MPF model. The discrete circles are from the calculations of Schoeck et al. [7]. (c) shows both configurations on the GSF energy surface (in units of mJ m^{-2}).

twist boundary. Construction of a twist boundary from a perfect crystal may be done in two consecutive steps: (a) a rigid-body rotation of the top half crystal with respect to the bottom half. The displacement due to the rotation is $\mathbf{u}_R$ (Fig. 2) and (b) local relaxation of both half crystals: an original point P in the boundary plane moves to T in the top crystal and to B in the bottom crystal, with displacements of $\mathbf{v}_T$ and $\mathbf{v}_B$, respectively. The relaxation displacements produce no macroscopic rotation of the crystal and, like the Peierls model, are assumed to be inelastic in the boundary plane and linear elastic in the remaining crystal. The total relative displacement between the two half crystals after the two steps is $\mathbf{u}_{BT}(\mathbf{r}) = \mathbf{v}_{BT}(\mathbf{r}) + \mathbf{u}_R(\mathbf{r})$.

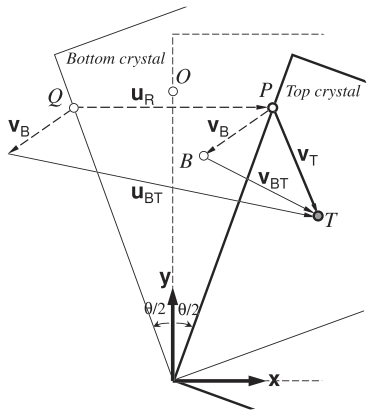

Fig. 2. Displacements in construction of a twist boundary.

Similar to the dislocation model, the energy of the twist boundary consists of a misfit energy (from the inelastic force in the boundary plane in 2-D),

$$E^m = E^m[\mathbf{u}_{BT}] = E^m[\mathbf{v}_{BT}(\mathbf{r}) + \mathbf{u}_R(\mathbf{r})] \tag{14}$$

and an elastic energy (from the two linear elastic half spaces in 3-D),

$$E^{el} = E^{el}[\mathbf{v}_{BT}(\mathbf{r})] \tag{15}$$

The displacement of the rigid-body rotation is

$$\mathbf{u}_R(\mathbf{r}) = [\mathbf{R}(\theta/2) - \mathbf{R}(-\theta/2)]\mathbf{r} \tag{16}$$

with $\mathbf{R}$ the rotation matrix

$$\mathbf{R}(\omega) = \begin{pmatrix} \cos\omega & \sin\omega \\ -\sin\omega & \cos\omega \end{pmatrix}$$

$\mathbf{u}_R$ is subtracted from the elastic energy (Eq. (15)) because a rigid-body rotation does not contribute to the elastic strain. Note that the remaining local relaxation displacement, $\mathbf{v}_{BT}$, is periodically varied on the grain boundary plane and can be solved by Eq. (9).

We apply the formulas (Eqs. (9), (11), (14) and (15)) to simulate the $(1\,1\,1)$-twist boundary of aluminum. The GSF and elastic constants of aluminum are from *ab initio* calculations. Each calculation is performed by imposing a fixed macroscopic rotation angle θ. The initial condition is

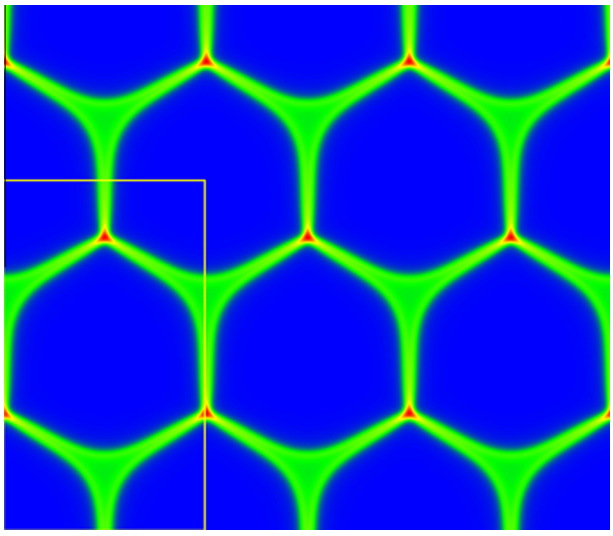

Fig. 3. Misfit energy plot of the (1 1 1) pure-screw twist boundary of Al ($\theta = 1°$). The bottom left box (size $57.3b \times 99.2b$) shows the periodic cell of computation.

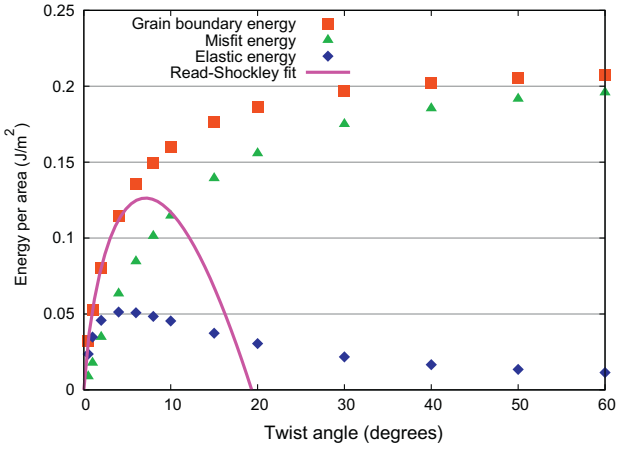

Fig. 4. Grain boundary energy.

$\mathbf{u}_{BT}(\mathbf{r}) = \mathbf{u}_{R}(\mathbf{r})$ (or $\mathbf{v}_{BT}(\mathbf{r}) = 0$ and a twist angle θ). Relaxation takes place until the variation of the total energy $\delta E/\delta \mathbf{v}_{BT}(\mathbf{r})$ reaches zero. A fully relaxed pure-screw twist boundary with twist angle $\theta = 1^{\circ}$ is shown in Fig. 3. The grain boundary energy is calculated for different twist angles up to 60°, plotted in Fig. 4.

4. Discussion

The twist boundary (Fig. 3) reproduces the well-known alternating contracted and extended nodes on a (1 1 1) plane of a face-centered cubic (fcc) crystal. However, this is now done quantitatively in a Peierls framework, without assumptions of the size of the nodes or the spacing and orientation of the constituent dislocation segments. On the other hand, since the present model is still formulated in a continuum space, the resultant grain boundary energies along the twist angle (Fig. 4) only reproduce the envelop of the actual curve without showing cusps that correspond to special boundary orientations. At small angles (<4°), the grain boundary may be considered as a structure formed by three distinctive arrays of $1/2\langle 1\,1\,0\rangle$ screw dislocations related by a threefold rotation. The dislocation density increases with the twist angle, as do the specific (i.e. per area) elastic energy and misfit energy. However, with further increasing angle, the specific elastic energy starts to decrease because of the overlapping of strain fields from neighboring dislocations, while the misfit energy continues to increase monotonically. At small angles, the grain boundary energy may be fitted with the Read–Shockley equation, $\gamma_s = \gamma_0\theta(A - \ln\theta)$, with $\gamma_0 = 1.0183\,J\,m^{-2}, A = -1.0868$. The latter corresponds to a cut-off radius $r_0/b = 1.28$. It is seen that the Read–Shockley equation fits up to only about 4°.

Real grain boundaries obviously consist of discrete atoms. Although the present model is formulated on a continuum basis, it is easy to see that, at small twist angles, because the period of the grain boundary structure (or the spacing between dislocations) L is much greater than the fcc lattice spacing, the grain boundary energy obtained by counting over discrete lattice (individual atomic bonds) is almost the same as by integrating continuously. At large angles, however, the difference will become significant. To a first approximation, we may take a grain boundary relaxed in the continuum model, but count the misfit energy only on fcc lattice points on the slip plane, and assume that the elastic energy is the same as in the continuum model. This is similar to the method Nabarro used to investigate the Peierls stress of a dislocation [1]. The resultant grain boundary energy is plotted in Fig. 5. It is interesting to see that, at $\theta = 60°$, the grain boundary energy by Nabarro-style discrete lattice sum [39] is very low. This is indeed physically reasonable, since $\theta = 60°$ is a coherent twin ($\Sigma 3$) boundary. We can understand this result by considering the facts that: (a) the energy associated with a long-wavelength, low-amplitude elastic strain field in the model is small because of the fine continuum dislocation network

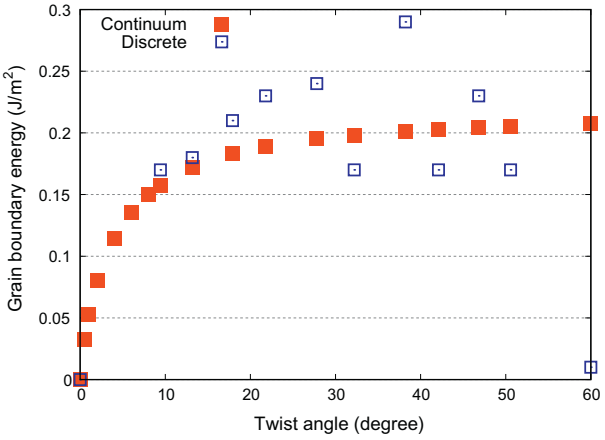

Fig. 5. Grain boundary energy calculated by a discrete sum over fcc lattice sites on the slip plane.

spacing L on the boundary, which leads to rapid exponential decay of the stress field away from the boundary, with decay length $\propto L$ and (b) the discrete lattice sampling of inelastic energy avoids the cores of the fine continuum dislocations. From Fig. 5, we see that a cuspy $\gamma(\theta)$ appears as soon as the Nabarro-style continuum integral $\rightarrow$ discrete lattice sum mapping is performed.

Thus, our modeling results demonstrate explicitly that the cuspy grain boundary energy $\gamma(\theta)$ seen experimentally has exactly the same physical origin as the Peierls lattice friction for dislocations. If one tries to continuously increase the twist angle θ of a grain boundary, one must encounter "Peierls torque friction" due to encountering the $\gamma(\theta)$ cusps, which exist at all crystallographic (integer Σ) twist angles, but with greatly varying magnitudes. The only difference from the Peierls stress for dislocations is that the former is for a rotational defect while the latter is for a translational defect, on a 2-D crystallographic plane.

5. Summary

By partitioning the total energy of a dislocation-containing crystal in the same way as in the Peierls model, we have shown that the MPF predictions of the core structure of straight dislocations agree well with the Peierls model. At the same time, we have demonstrated that the MPF model is a 3-D generalization of the Peierls model, and that it is able to predict the structure and energy of more complicated dislocation substructures formed, for example, at grain boundaries or inter-phase interfaces, using solely *ab initio* calculation inputs. The application of the MPF model has generated immediately non-trivial results. It shows that, for a pure-screw twist boundary that has a well-defined dislocation substructure, the Read–Shockley equation is valid up to only 4°. It predicts cusps for high-angle special grain boundaries and Peierls torque friction for grain boundary sliding that has the same physical origin as the Peierls–Nabarro lattice friction for dislocation glide.

Acknowledgements

We thank Professor Gunther Schoeck for kindly providing Ni_3Al GSF energy data and the program for computing Peierls's solution of dislocation core profiles. Y.W. acknowledges support by DOE DE-SC0001258 and NSF DMR-1008349. J.L. acknowledges support by NSF DMR-1240933 and DMR-1120901.

References

[1] Hirth JP, Lothe J. Theory of dislocations. 2nd ed. New York: Wiley; 1982.
[2] Sutton AP, Balluffi RW. Interfaces in crystalline materials. Oxford University Press; 1997.
[3] Earmme YY, Weiner JH. Loss-free dislocation motion in a lattice model. Phys Rev Lett 1974;33(26):1550–2.
[4] Flytzanis N, Crowley S, Celli V. Solitonlike motion of a dislocation in a lattice. Phys Rev Lett 1977;39(14):891–4.
[5] Bulatov VV, Kaxiras E. Semidiscrete variational Peierls framework for dislocation core properties. Phys Rev Lett 1997;78(22):4221–4.
[6] Jos B, Duesbery MS. The Peierls stress of dislocations: an analytic formula. Phys Rev Lett 1997;78(2):266–9.
[7] Schoeck G, Kohlhammer S, Fhnle M. Planar dissociations and recombination energy of [1–10] superdislocations in ni3al: generalized peierls model in combination with ab initio electron theory. Philos Mag Lett 1999;79(11):849–57.
[8] Ismail-Beigi S, Arias TA. Ab initio study of screw dislocations in mo and ta: a new picture of plasticity in bcc transition metals. Phys Rev Lett 2000;84:1499.
[9] Lu G, Zhang Q, Kioussis N, Kaxiras E. Hydrogen-enhanced local plasticity in aluminum: an ab initio study. Phys Rev Lett 2001;87(9):095501.
[10] Rosakis P. Supersonic dislocation kinetics from an augmented Peierls model. Phys Rev Lett 2001;86(1):95–8.
[11] Lu G, Kaxiras E. Can vacancies lubricate dislocation motion in aluminum? Phys Rev Lett 2002;89(10):105501.
[12] Woodward C, Rao SI. Flexible ab initio boundary conditions: simulating isolated dislocations in bcc mo and ta. Phys Rev Lett 2002;88:216402.
[13] Woodward C, Trinkle DR, Hector Jr LG, Olmsted DL. Prediction of dislocation cores in aluminum from density functional theory. Phys Rev Lett 2008;100(4):045507.
[14] Hirth JP. A brief history of dislocation theory. Metall Trans A 1985;16(12):2085–90.
[15] Peierls R. The size of a dislocation. Proc Phys Soc Lond 1940;52:34–7.
[16] Wang Y, Li J. Phase field modeling of defects and deformation. Acta Mater 2010;58(4):1212–35.
[17] Lepinoux J, Kubin LP. The dynamic organization of dislocation-structures – a simulation. Scripta Metall 1987;21(6):833–8.
[18] Gulluoglu AN, Srolovitz DJ, Lesar R, Lomdahl PS. Dislocation distributions in 2 dimensions. Scripta Metall 1989;23(8):1347–52.
[19] Amodeo RJ, Ghoniem NM. Dislocation dynamics. 1. A proposed methodology for deformation micromechanics. 2. Applications to the formation of persistent slip bands, planar arrays and dislocation cells. Phys Rev B 1990;41(10):6958–76.
[20] van der Giessen E, Needleman A. Discrete dislocation plasticity – a simple planar model. Model Simulat Mater Sci Eng/ 1995;3(5):689–735.
[21] Zbib HM, Rhee M, Hirth JP. On plastic deformation and the dynamics of 3D dislocations. Int J Mech Sci 1998;40(2–3):113–27.
[22] Bulatov V, Abraham FF, Kubin L, Devincre B, Yip S. Connecting atomistic and mesoscale simulations of crystal plasticity. Nature 1998;391(6668):669–72.
[23] Devincre B, Hoc T, Kubin L. Dislocation mean free paths and strain hardening of crystals. Science 2008;320(5884):1745–8.
[24] Weygand D, Poignant M, Gumbsch P, Kraft O. Three-dimensional dislocation dynamics simulation of the influence of sample size on the stress–strain behavior of fcc single-crystalline pillars. Mater Sci Eng A – Struct Mater Prop Microstruct Process 2008;483:188–90.
[25] Vitek V. Intrinsic stacking faults in body-centred cubic crystals. Philos Mag 1968;18(154):773–&.
[26] Kaxiras E, Duesbery MS. Free-energies of generalized stacking-faults in si and implications for the brittle-ductile transition. Phys Rev Lett 1993;70(24):3752–5.
[27] Zimmerman JA, Gao HJ, Abraham FF. Generalized stacking fault energies for embedded atom fcc metals. Model Simulat Mater Sci Eng 2000;8(2):103–15.
[28] Ogata S, Li J, Yip S. Ideal pure shear strength of aluminum and copper. Science 2002;298(5594):807–11.
[29] Mackenzie JK. The stresses and energies associated with inter-crystalline boundaries. Proc Phys Soci Lond Sect A 1950;63(372):1370.

[30] Wang YU, Jin YM, Cuitino AM, Khachaturyan AG. Nanoscale phase field microelasticity theory of dislocations: model and 3D simulations. Acta Mater 2001;49:1847–57.
[31] Khachaturyan AG. Some questions concerning the theory of phase transformations in solids. Sov Phys Solid State 1967;8:2163.
[32] Khachaturyan AG, Shatalov GA. Elastic interaction potential of defects in a crystal. Sov Phys Solid State 1969;11:118.
[33] Khachaturyan AG. Theory of structural transformations in solids. New York: John Wiley & Sons; 1983.
[34] Shen C, Wang Y. Phase field model of dislocation networks. Acta Mater 2003;51(9):2595–610.
[35] Shen C, Wang Y. Incorporation of gamma-surface to phase field model of dislocations: simulating dislocation dissociation in fcc crystals. Acta Mater 2004;52(3):683–91.
[36] Wang S. Lattice theory for structure of dislocations in a two-dimensional triangular crystal. Phys Rev B 2002;65(9):094111. pRB.
[37] Hillert M. A theory of nucleation of solid metallic solutions. Ph.D. thesis. Massachusetts Institute of Technology; 1956.
[38] Cahn JW, Hilliard JE. Free energy of a nonuniform system. I. Interfacial free energy. J Chem Phys 1958;28(2):258–67.
[39] Nabarro FRN. Dislocations in a simple cubic lattice. Proc Phys Soc Lond 1947;59:256–72.